Hyperfine frequency shift and Zeeman relaxation in alkali-metal-vapor cells with antirelaxation alkene coating

Eric P. Corsini,[1,*] Todor Karaulanov,[1] Mikhail Balabas,[2,3] and Dmitry Budker[1,4,†]
[1]*Department of Physics, University of California, Berkeley, California 94720-7300, USA*
[2]*S. I. Vavilov State Optical Institute, St. Petersburg 199034, Russia*
[3]*Faculty of Physics, Ulyanovskaya 3, Saint Petersburg State University, St. Petersburg 198504, Russia*
[4]*Nuclear Science Division, Lawrence Berkeley National Laboratory, Berkeley California 94720, USA*
(Received 13 January 2012; revised manuscript received 15 June 2012; published 14 February 2013)

An alkene-based antirelaxation coating for alkali-metal vapor cells exhibiting Zeeman relaxation times up to 77 s was recently identified by Balabas *et al*. The long relaxation times, two orders of magnitude longer than in paraffin- (alkane-) coated cells, motivate revisiting the question of what the mechanism is underlying wall-collision-induced relaxation and renew interest in applications of alkali-metal vapor cells to secondary frequency standards. We measure the width and frequency shift of the ground-state hyperfine $m_F = 0 \rightarrow m'_F = 0$ transition (clock resonance) in vapor cells with ^{85}Rb and ^{87}Rb atoms, with an alkene antirelaxation coating. We find that the frequency shift is slightly larger than for paraffin-coated cells and that the Zeeman linewidth scales linearly with the hyperfine frequency shift.

DOI: 10.1103/PhysRevA.87.022901 PACS number(s): 34.35.+a, 06.20.fb, 06.30.Ft, 32.10.Fn

I. INTRODUCTION

Important experiments in fundamental physics and applications in metrology, such as magnetometry and time and frequency standards, rely on long-lived ground-state polarization of alkali vapors [1,2]. The major technical difficulty is to preserve atomic polarization while containing the vapor. Buffer gas or antirelaxation coated glass cells and laser cooling and trapping are the current leading techniques. Glass cells filled with an alkali vapor at near-room temperature are easier to implement than laser trapping. For applications to magnetometry and secondary frequency standards, antirelaxation coated cells have the additional benefit of lower laser power requirements; they also benefit from motional averaging which reduces the magnetic-field-gradient resonance broadening [3].

Coating the cell walls with paraffin was proposed by Ramsey in 1950 [4], first realized by Robinson and Dehmelt in 1958 [5], and extensively characterized by Bouchiat and Brossel [6,7]. The coating consists of a thin film of long chains of nominally saturated C–C bond alkane molecules (C_nH_{2n+2}) [8]. Octadecyltrichlorosilane (OTS), which allows approximately 2000 polarization-maintaining wall bounces at temperatures up to 170 °C, and paraffin, with up to 10 000 bounces (but limited to below 60 to 80 °C), have been the leading antirelaxation coatings in the last several decades [8,9]. There is limited understanding about the interaction of paraffin with alkali atoms and why only certain procedures by which the coating is applied work, which up to now has made the production of high-quality cells more an art than a science [10].

Alkene (C_nH_{2n+1}) coatings [11] with one unsaturated C=C bond were recently demonstrated [12]. They allow up to 10^6 bounces with atoms in the ground state and enable Zeeman-coherence lifetimes (in a ∼1 inch spherical cell) to reach from several seconds to over one minute (up to two orders of magnitude improvement over paraffin). This discovery renewed the interest in understanding the underlying mechanism in wall-collision-induced decoherence and prompted the question: "Is a long relaxation time due to a short cell-wall adsorption (dwelling) time?" A short wall-dwelling time would imply a small hyperfine frequency shift (Sec. III). It would reignite interest in vapor-coated cells for use in applications to secondary frequency standards, an application that has been limited by the large, temperature-dependent frequency shift of the hyperfine $m_F = 0 \rightarrow m'_F = 0$ transition (clock resonance) [13].

To answer the above question we measure the width and frequency shift of the clock resonance in alkali-metal vapor cells with alkene-based antirelaxation coatings. We compare our results to those with alkane-coated vapor cells [14] and propose an explanation for the result and the source of wall-collision-induced relaxation.

II. ANTIRELAXATION COATED CELLS

A. Background

Atom-wall collision processes, a subset of surface-interaction science, are ubiquitous in nature and yet are far from being well understood. Upon collision with a surface, an atom (or molecule) undergoes physical adsorption (physisorption—in contrast to chemical adsorption which is called chemisorption) by the wall potential (the result of a surface-induced electric field), adheres to and desorbs from the surface after an average adsorption time $\bar{t}_w$, with an Arrhenius temperature dependence [15–18]

$$\bar{t}_w = \tau_o e^{E_w/kT}, \quad (1)$$

where τ_o is the period of vibration of the adsorbed atom in the wall potential, E_w is the adsorption energy, k is the Boltzmann constant, and T is the temperature.

While on the surface, the adsorbed atom undergoes surface migration [19]. In the limit of a perfectly smooth surface adsorption energy, the adsorbed atoms form a two-dimensional gas governed by the atoms' thermal kinetic energy

*eric.corsini@gmail.com
†http://budker.berkeley.edu/

transverse to the surface. The two-dimensional mean-free path is generally smaller, and the density larger, than for the three-dimensional gas [19]. When there are spatial fluctuations in the adsorption energy E_w, the mean-free path becomes even shorter due to the participation of surface atoms (this mechanism is also the one by which energy is exchanged between the adsorbed atoms and the surface [19]). In the limit when the average fluctuation ΔE_w is of the order of the atoms' kinetic energy, an atom hops from one adsorption site to another with a characteristic time

$$\bar{t}_{hop} = \tau_o e^{\Delta E_w/kT}. \quad (2)$$

The property of a good antirelaxation coating is thought to come from the absence of free electron spins which could result in alkali-metal spin destruction, and from a low dielectric constant (low polarizability) and consequently a low adsorption energy E_w, which reduces the time of adsorption $\bar{t}_w$ [Eq. (1)]. For example, paraffin and Pyrex have a wall adsorption energy of the order of 0.1 eV [6] and 0.5 eV [17], respectively.

Additionally, a small average spatial fluctuation ΔE_w in the coating's adsorption energy may play a central role in determining the antirelaxation quality of the coating (Sec. VII A).

B. Previous work and techniques for measuring the adsorption energy and adsorption time

Ingenious methods have been realized to measure the time of adsorption $\bar{t}_w$, which is one of the most consequential variables of surface interaction.

In one of the earliest attempts in the 1930s, Clausing [20,21] directly measured the average propagation time $\bar{t}$ of argon atoms through a glass capillary. Molecular flow (Knudsen flow) transit time through a capillary can be calculated and decoupled from surface interaction (for example, the average propagation time of an atom through a 1-μm-diameter, 1-m-long capillary, with a 100 μs average adsorption time, is 50 s, compared to 5 ms without adsorption). Clausing derived the time of adsorption $\bar{t}_w = (2d^2/l^2)\bar{t} - d/\bar{v}$, where d and l are the capillary diameter and length, $\bar{v}$ is the average atomic thermal velocity, and found $\bar{t}_w = 31$ μs for a glass surface at 90 K.

In 1964 Bouchiat and Brossel [6,7] measured the adsorption energy and time of adsorption by measuring the Zeeman relaxation time as a function of magnetic field. When scanning the magnetic field, Bouchiat and Brossel observed steps (magnetic decoupling) in the Zeeman relaxation time. A step occurs when the frequency corresponding to the adsorbed atoms' Zeeman splitting reaches the inverse correlation time of a perturbing wall magnetic field. Each Zeeman relaxation process reveals itself as a step; one in particular involves the average time $\bar{t}_w$ that an atom spends on one adsorption site.

In 1986, Liberman and Knize [22] quantified the adsorption energy and the lifetime of an atom in the vapor by measuring the alkali-metal vapor density as a function of temperature in a coated vapor cell with a reservoir. The results showed that the coatings acts as a long-term pump of the alkali-metal atoms.

In 1994 Stephens *et al*. [19] quantified the adsorption energy by measuring the vapor density in a cell with a fixed number of atoms as a function of temperature. They also detected the time of adsorption by measuring the vapor density in a cell filled with alkali-metal atoms as a function of time. The measurements were realized in the context of atom trapping and interaction between cesium atoms and Pyrex, stainless steel, sapphire, and OTS.

In 2004 Brewer *et al*. [23] measured the energy and time of adsorption by light induced atomic desorption (LIAD), a technique pioneered by Moi and Gozzini *et al*. [24,25]. This process involves atom desorption through nonresonant photon stimulation. The measurements were made with sodium and rubidium atoms and a polydimethylsiloxane (PDMS) coating and showed that desorption is a multistep process in which the initial excitation is decoupled from the final desorption. In 2009 Karaulanov *et al*. extended the investigation of LIAD into the UV range and found a sharp dependence on wavelength [26]. That investigation was made with alkali-metal vapors and paraffin coatings. The results derived from LIAD underline the complex dynamics governing adsorption.

In 2005 Budker *et al*. [14] indirectly measured the time of adsorption by measuring the shift in the clock resonance frequency caused by the adsorption energy of the cell-wall coating (cell-wall hereafter). The measurements were made with alkali-metal atoms and paraffin- and paraflint- (alkane molecules) coated cells.

In 2009 Zhao *et al*. [27] directly measured the time of adsorption by means of Zeeman light shift of polarized alkali-metal atoms pumped and probed by evanescent waves. The work concerned interaction of alkali-metal atoms with OTS and paraffin [27,28].

In 2012 Balabas and Tret'yak [29] made a detailed investigation (and proposed a model) of the dynamics of alkali-metal atoms in the vapor phase with the coating, in a cell with a lockable reservoir (stem lock).

This summary, although not exhaustive, highlights the continuing interest and new techniques in adsorption-science research. The ongoing research and the newer techniques of evanescent waves [27,28] and LIAD [23–26] are revealing adsorption dynamics far more complex than that described early on by Eq. (1). More recent works by Zhao *et al*. [27,28], by Liberman and Knize, by Balabas *et al*. [22,29,30], by Freitas *et al*. [31], by Zhang, by Seebauer *et al*. [32], and work with LIAD [23–26] indicate that in addition to the two-dimensional (surface) adsorption (with typical correlation time of the order of 10^{-9} s; see Sec. III A), adsorption also involves effects pertaining to surface defects and atoms entangled in the bulk of the coating (for times spanning several orders of magnitude longer) and exhibiting a non-Arrhenius character.

III. THEORY

A. Hyperfine resonance frequency shift

The adsorption energy E_w has two related effects in antirelaxation coated vapor cells. The first effect is physical adsorption of the alkali-metal atoms, as described in Sec. II A. The second effect is a shift ΔE_{hf} in the hyperfine ground-state energy levels during physical adsorption. A similar hyperfine energy shift is observed with alkali-metal atoms in the presence of foreign gases [33]. The hyperfine energy shift is a function of the adsorption energy,

$$\Delta E_{hf} = f(E_w), \quad (3)$$

and is scaled by the average time $\bar{t}_w$ that the atoms spend on the wall relative to the average time between collisions with the walls $\bar{t}_c$ and leads to an average ground-state hyperfine frequency shift,

$$\Delta\nu = \frac{\bar{t}_w}{\bar{t}_w + \bar{t}_c}\frac{\Delta E_{hf}}{h}, \tag{4}$$

where h is Planck's constant.

Assuming the trajectories of the atoms have a cosine angular distribution after desorption ([16] Appendix 3B–C), the atoms' average collision rate per unit surface is

$$\nu_c = \frac{1}{4}\frac{N}{V}\bar{v}, \tag{5}$$

where N is the number of atoms in a volume V, $\bar{v} = \sqrt{8kT/(\pi M)}$ is the average atomic thermal velocity, k is the Boltzmann constant, and M the mass of the atom. For one atom, the average collision rate with a wall surface of area S is

$$\nu_c = \frac{1}{4}\frac{S}{V}\bar{v}, \tag{6}$$

and for a spherical cell the average time between collisions is

$$\bar{t}_c = \frac{4R}{3\bar{v}}, \tag{7}$$

where R is the radius. For nonspherical cells, R can be generalized to be the cell's geometric factor; a function of both surface area and volume (shape and size).

In the present work and in the work of Ref. [14] the cell-wall-dwelling times of different cells are evaluated by measuring the hyperfine frequency shift and scaling it to a common cell size, temperature, and alkali-metal species. The underlying assumption is that the hyperfine energy shift is nearly constant so that the hyperfine frequency shift has the same linear dependence on the wall-dwelling time in all cells. One may ask "is this a reasonable assumption?"

For $\bar{t}_w \ll \bar{t}_c$ and from Eq. (4) we have

$$|\Delta\nu| \propto \Delta E_{hf}\frac{\bar{t}_w}{\bar{t}_c}, \tag{8}$$

which means that to measure hyperfine frequency shifts ($\Delta\nu$), in order to compare cell-wall adsorption energies E_w between alkane coatings (work in Ref. [14]), between alkane and alkene coatings, and between alkene coatings (present work) by only measuring the hyperfine frequency shift [14], one must assume from Eq. (8) that ΔE_{hf} is nearly the same for all alkane- and alkene-coated cells. One needs to assess the quality of that assumption for coatings differing in their molecular structure and for coatings with the same molecular structure but with Zeeman relaxation times T ranging from several seconds to over one minute.

Bouchiat and Brossel measured the cell-wall-dwelling time $\bar{t}_w \simeq 10^{-9}$ s in paraffin-coated cells using magnetic decoupling (see Ref. [6] and Sec. II B). This measurement implies that for a hyperfine frequency of $\nu = 3.6$ GHz (^{85}Rb), for a typical hyperfine frequency shift $\Delta\nu = -100$ Hz, in a cell of radius $\sim$2 cm, at room temperature ($\bar{t}_c \simeq 10^{-4}$ s), and from Eq. (4),

$$\frac{\Delta E_{hf}}{E_{hf}} = \frac{\Delta\nu}{\nu}\frac{\bar{t}_w + \bar{t}_c}{\bar{t}_w} \simeq 0.3\%. \tag{9}$$

Consequently, the hyperfine energy shift ΔE_{hf} caused by the cell-wall potential is within the limit of applicability of perturbation theory and we may expect Eq. (3) to be a linear relationship ($\Delta E_{hf} \propto E_w$).

From Eq. (1), we have $t_w \propto e^{E_w}$, which implies that substantial changes in t_w can be associated with small changes in E_w (and therefore small changes in the hyperfine energy shift ΔE_{hf}), and that presuming that the hyperfine energy shift is nearly constant, so as to interpret the hyperfine frequency shift as a measure of cell-wall-dwelling time, "is a reasonable assumption."

A different adsorption mechanism in which the atoms are thought to be trapped inside the tangled web of the long paraffin molecules (C_nH_{2n+2} where $n = 40$ to 60) on the cell wall was the model proposed by Balabas *et al.* [30] and by Ulanski and Wu [28] who measured a dwelling time $\bar{t}_w \simeq 10^{-6}$ s in a paraffin-coated cell with 5 torr of nitrogen buffer gas.

The large cell-wall-dwelling-time difference between the results of Bouchiat and Brossel [6] and of Ulanski and Wu [28] (three orders of magnitude difference) may be that the former work pertains to a population of atoms interacting with the coating's surface, whereas the latter work pertains to another population of atoms interacting with the bulk of the coating. Moreover, the results in Refs. [22,29–32] and with LIAD [23–26] point to a third population of atoms which is near-permanently trapped in the coating. Information on the respective sizes of atom populations may be contained in the results from Bouchiat and Wu, and the works in Refs. [22,29,30], and with LIAD. In fact there may be a continuum of dwelling times ranging from nanosecond (Bouchiat's measurements) to near-permanent. In this work we assume that the population of atoms trapped in the coating does not significantly contribute to the hyperfine energy shift ΔE_{hf}; we assume that atoms dwelling at the surface of the cell wall, as described by Bouchiat and Brossel [6], make the population of atoms generating the hyperfine frequency shift.

B. Hyperfine resonance linewidth

In addition to the hyperfine frequency shift, another measurable independent quantity is the width of the hyperfine transitions Γ_{hf}. The linewidth comes from two main known sources. The first source is spin exchange (between atoms in the vapor and in the two hyperfine ground states):

$$\frac{\Gamma_{se}}{2\pi} = \frac{\mathcal{R}(I)n\bar{v}_{rel}\sigma_{se}}{\pi}, \tag{10}$$

where $\mathcal{R}(I) = (6I + 1)/(8I + 1)$ (see Sec. VI of Ref. [34]) is the nuclear slow-down factor in the low polarization limit, I is the nuclear spin, n is the atomic density, $\bar{v}_{rel}$ is the average relative velocity of the colliding atoms, and σ_{se} is the spin cross section.

The second source is the adiabatic broadening Γ_a which is the result of the statistical nature of $\bar{t}_w$ and $\bar{t}_c$ which leads to a dispersion of the average phase shift $\bar{\Phi}_w$ accumulated by the atoms at each adsorption event [14],

$$\frac{\Gamma_a}{2\pi} = \frac{\bar{\Phi}_w{}^2}{\pi\bar{t}_c}. \tag{11}$$

Other sources of relaxation (assumed to be small in this work), include the stem effect, in which atoms are re-adsorbed by the alkali-metal reservoir, and coating absorption-effect, in which the atoms are trapped inside the coating's long molecule chains [14].

For hyperfine frequency shifts $\Delta\nu$, which in this work are of the order of $\simeq -100$ Hz, Γ_a ($\propto\bar{\Phi}_w{}^2$) is the dominating contribution [as visualized in Fig. 4(a)] giving the total hyperfine linewidth a near-quadratic dependence in the variable $\bar{\Phi}_w$.

In contrast, the hyperfine frequency shift

$$\Delta\nu = \frac{1}{2\pi}\frac{\bar{\Phi}_w}{t_c} = \frac{3}{8\pi}\frac{\bar{\Phi}_w}{R}\bar{v} \tag{12}$$

is linear in $\bar{\Phi}_w$ [14].

Measuring Γ_a [Eq. (11)] is an independent measurement of $\bar{\Phi}_w$ which, if inconsistent with the one derived from measuring $\Delta\nu$ [Eq. (12)] would indicate the presence of additional relaxation mechanisms.

C. Zeeman linewidth

In this work we measure the Zeeman longitudinal resonance linewidth $1/T_1$, which, in contrast to the hyperfine resonance, is not sensitive to adiabatic collisions. T_1 (Sec. V) is sensitive to spin randomization on the wall (nonadiabatic collisions) and to uniform sources of relaxation, such as collisions with the alkali-metal in the stem reservoir and semipermanent absorption by the cell-wall coating [35,36].

IV. EXPERIMENTAL SETUP

The apparatus is shown in Fig. 1. The components used in this work consist of an alkali-metal vapor cell with an alkene-based antirelaxation coating, a four-layer mu-metal shield, a temperature stabilizing mechanism, a coil-system to provide a homogeneous bias magnetic field, a microwave loop antenna, a laser, and a photodiode to measure the laser-light transmission through the cell.

The pump-probe beam is from a distributed feedback (DFB) laser (Toptica LD-0795) resonant with the rubidium (Rb) $5^2S_{1/2}$–$5^2P_{1/2}$ (D_1 line, $\lambda = 795$ nm).

The 3-mm-diameter collimated laser beam passes through an isolator, a variable neutral density filter, a polarizer, a rotatable quarter-wave plate, and the alkali-metal-vapor cell. The photodiode signal is amplified (SR-560) and the amplitude is digitized with a digital acquisition system (DAQ - IOtech P-DAQ/3001).

A dichroic atomic vapor laser lock (DAVLL) [37] is used to lock the laser optical frequency near the peak of the $F = 2 \rightarrow F' = 1$ transition for ^{87}Rb and the $F = 3 \rightarrow F' = 2$ transition for ^{85}Rb, for maximum hyperfine resonance contrast. A temperature controller (Omega CNI3252) maintains the DAVLL vapor-cell temperature at $\sim$50 °C to increase the electronic-feedback signal-to-noise ratio.

A reference cell and a Fabry-Pérot interferometer provide additional monitoring of the optical frequency stability.

The magnetic field is applied with a set of three orthogonal coils, three gradient coils (applying magnetic-field gradients along the same three orthogonal directions), and one longitudinal second-order gradient coil, positioned within the innermost layer of the four-layer mu-metal shield manufactured in part by Amuneal. COMSOL multiphysics modeling was used to optimize the geometry of the coils and achieve better than 1% magnetic-field homogeneity within a 2-inch-diameter, 4-inch-long cylindrical volume.

A 3.6 mG bias magnetic field resolves the $m_F = 0 \rightarrow m_{F'} = 0$ (0-0) rubidium clock resonance from the other Zeeman components of the hyperfine resonance (Fig. 2). The clock resonance is only sensitive to second-order magnetic-field-induced hyperfine frequency shift, which is negligible in this work. There are seven Zeeman components for ^{87}Rb and eleven for ^{85}Rb.

The pump-light polarization and the relative orientations of the pump light, magnetic field, and microwave field are optimized for optimum hyperfine resonance contrast. Maximum contrast is achieved with the axis of the antenna oriented approximately parallel to the shield's axis, with the magnetic-field orientation tilted approximately 10° upward, and with the pump light polarization made approximately linear.

The microwave magnetic field is generated by mixing the output of a synthesizer (HP8673B), set at a fixed frequency, and the output of a function generator (BNC625), whose frequency is swept through the desired measurement range. The function generator also outputs a marker step as an additional frequency reference. The mixer (Mini-Circuits ZX05-153) feeds a circulator (DiTom D3C6012). One port of the circulator is directed to a one-loop 2-cm-diameter antenna positioned next to the cell; the other port directs the return signal to a spectral analyzer (Agilent 8562F) to monitor the microwave frequency and power. A second microwave antenna serves as a receiver and provides an additional microwave-power monitor. The HP synthesizer, BNC function generator, and Agilent spectral analyzer are referenced to a 10 MHz signal from a commercial wireless-network-referenced rubidium atomic clock (Symmetricom TS2700B).

A temperature controller (Omega CN77353-PV) regulates the DC current to two electric heaters consisting of quad-twisted nonmagnetic heater wire (Lake Shore QT36), positioned fore and aft of the cell and coiled along the main shield axis. The residual magnetic field produced by the heaters is on the order of 1 μG and can be neglected. The electric heaters are supplemented with a water heating and cooling system. The innermost shield serves to conduct and distribute the heat so as to achieve a temperature which is approximatively uniform within the cell's volume within a range of 15 to 50 °C.

V. MEASUREMENT PROCEDURES

Measurements were made on six rubidium (Rb) vapor cells. Four cells are coated with alkene Alpha Olefin Fraction C20-24 from Chevron Phillips (CAS Number 93924-10-8) with a light fraction removed by partial vacuum evaporation at 80 °C. One cell is coated with alkene AlphaPlus C30+ from Chevron Phillips (CAS Number 131459-42-2), and one cell is coated with deuterated paraffin. The melting temperature for C20-24 is 35 °C and is 73 °C for C-30. The cells are of different sizes, have cylindrical or spherical shapes, and are filled with enriched ^{87}Rb or with rubidium in natural isotopic abundance. They are prepared according to the technique described in Ref. [39]. The alkene-coated cells are fitted with a precision-ground stem lock [12,26] which nearly eliminates Zeeman relaxation caused by the atoms being reabsorbed by the

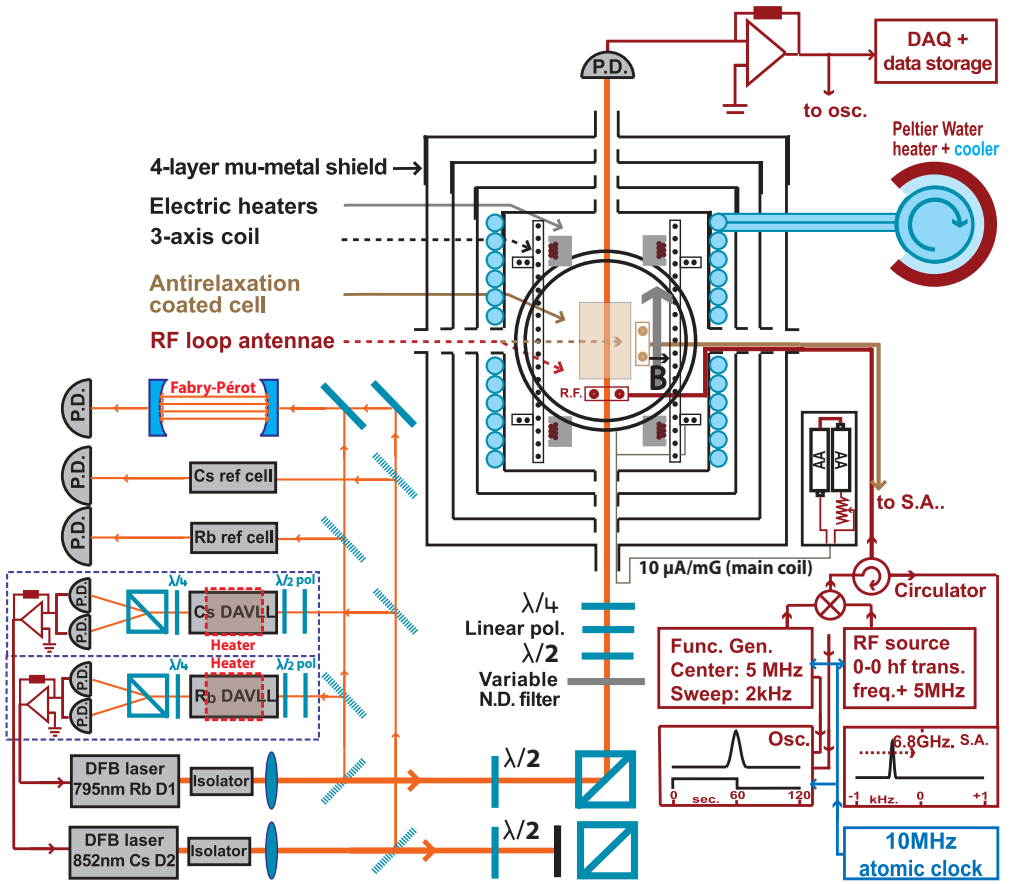

FIG. 1. (Color online) Apparatus: the alkene-coated cell is placed inside a four-layer mu-metal shield. A one-loop microwave antenna is positioned next to the cell. The orthogonal 3-axis coils and three gradient coils along the same axes induce an ∼3.6 mG bias magnetic field to resolve the Zeeman components of the hyperfine resonance. The magnetic-field axis is slightly tilted with respect to the axial symmetry to achieve optimum clock-resonance contrast. A synthesizer provides a fixed microwave source set 5 MHz above the hyperfine transition and is mixed with the output of a function generator whose frequency is swept through a 2 kHz span about a 5 MHz center frequency. A circulator directs the mixed output to the first one-loop microwave antenna and directs the return signal to a spectral analyzer (S.A.). The second one-loop antenna (when connected to the S.A.) serves to monitor the microwave power next to the cell. The inner-shield temperature stabilization is realized with two electric heaters consisting of quad-twisted nonmagnetic wire coiled in two solenoids parallel to the main axial symmetry and supplemented with a water heating and cooling system. The light beam from a distributed feedback (DFB) laser, is resonant with the rubidium (Rb) D_1 line, and is nearly linearly polarized, with approximately 5% circularity for optimum resonance contrast. Also for maximum contrast, the optical frequency is locked to the blue-detuned side of the peaks of $F = 2 \rightarrow F' = 1$ (^{87}Rb) and $F = 3 \rightarrow F' = 2$ (^{85}Rb), using a dichroic atomic vapor laser lock (DAVLL) [37]. Stability of the laser optical frequency is monitored with a reference (noncoated) cell and a Fabry-Pérot cavity. A photodiode registers the light transmission through the cell, and the signal is amplified, sampled, and recorded with a digital acquisition system (DAQ). [Note: the apparatus is a multipurpose platform (Chapters 5 and 6 of Ref. [38] show the complete range of configurations) designed to be used separately or in conjunction with a field-able multipurpose magnetometer platform (Chapter 4 of Ref. [38]), to investigate areas of atomic magnetometry and secondary frequency standards.]

stem reservoir (stem effect [6]). The Zeeman population lifetimes T_1 of the four C20-24 alkene-coated cells were measured with the stem lock closed and were found to range from 3 to 53 s. T_1 was measured using a modification of Franzen's "relaxation in the dark" technique [40], described in Ref. [35]. That technique yields two exponential decay constants characterizing the Zeeman population relaxation; the longer time constant is used to define T_1.

The microwave synthesizer was set 5 MHz above the rubidium hyperfine transition frequency, and the function generator frequency was centered at ∼5 MHz, such that the center of the sweep was approximately 100 Hz below the hyperfine transition to help in the data fit. The mixer output frequency, resonant with the hyperfine transition, was the difference frequency and was separated from the conjugate (sum) frequency by 10 MHz, and it was not low-pass filtered. At saturation power the off-resonant microwave magnetic field induced a 0-0 hyperfine transition ac Stark shift of approximately 10^{-5} Hz, which was neglected.

We measured the ground-state hyperfine $m_F = 0 \rightarrow m'_F = 0$ transition (clock resonance) width and frequency shift by sweeping the function generator frequency through a span of 2 kHz in a time of 120 s. The measurements were made for a range of microwave powers spanning 30 dB such that, at maximum microwave power, the width of the resonance was broadened by a factor of ∼5, and for optical powers ranging

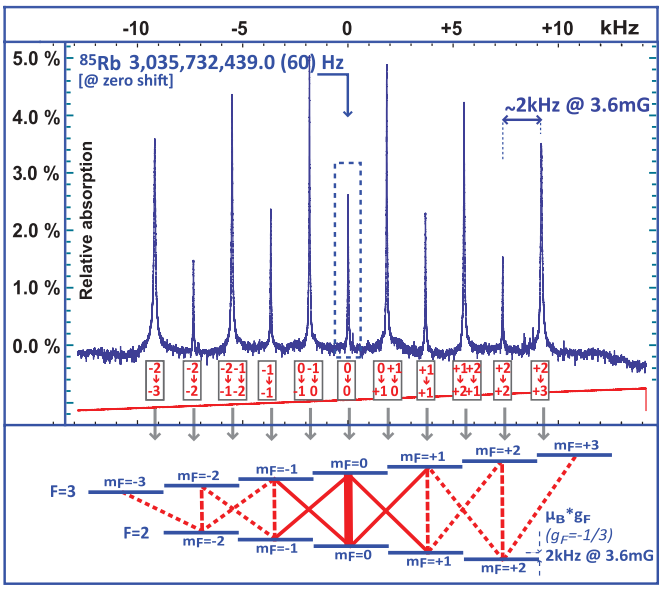

FIG. 2. (Color online) Upper panel shows the eleven Zeeman components of the hyperfine resonance in ^{85}Rb resolved with a ~3.6-mG-bias magnetic field. The relative intensities of the peaks depend on the relative orientation of the pump-light beam, the bias magnetic and microwave fields, the pump-light detuning, and the pump-light polarization. Under typical conditions the optical resonant absorption through the alkali-metal vapor is ~25% and increases by 1% to 5% on the hyperfine resonances. Lower panel shows the Zeeman sublevels for the hyperfine ground states $F = 2$ and $F = 3$ for ^{85}Rb, and the corresponding Zeeman components of the hyperfine transition.

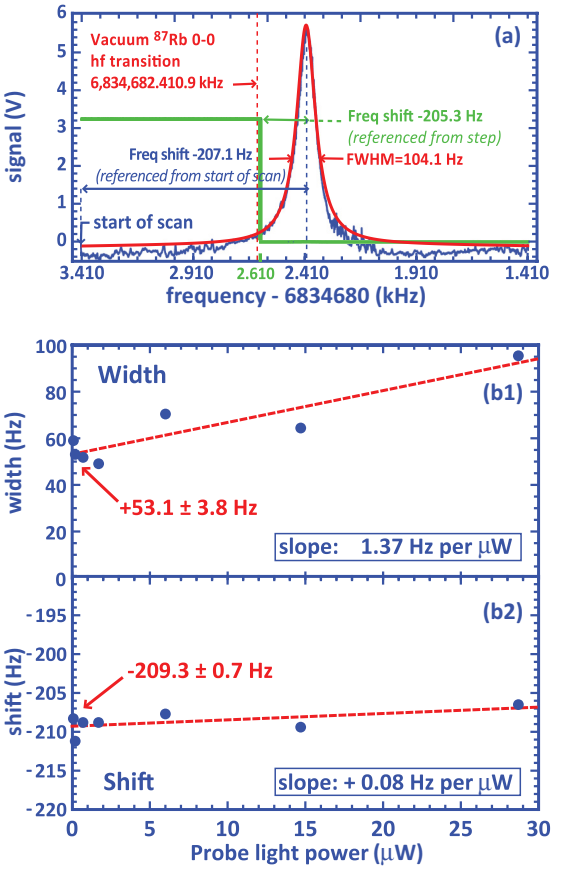

FIG. 3. (Color online) Example of how the $m_F = 0 \rightarrow m'_F = 0$ hyperfine transition ([0-0] - clock resonance) width and frequency shift are extracted. Panel (a) shows the scan of a ^{87}Rb clock resonance at large optical (10.7 μW) and microwave powers. The data are fit to a Lorentzian. The difference between the data and the wings of the fit may be attributed to imperfections in the measurement (see Sec. VI). The induced error in determining the resonance center frequency is within the margin of measurement error. To mitigate timing jitter the center frequency is measured from both the marker-step and from the beginning of the scan. In this example the clock-resonance unscaled (Sec. V) full width at half maximum (FWHM) and unscaled frequency shift, relative to the hyperfine frequency for atoms in free space, are 104 and −206 Hz (average of the measurement referenced to the marker-step and of the measurement from the start of the scan), respectively. Panels (b)(1) and (b)(2) show the extraction of the clock-resonance width and frequency shift by extrapolation to zero light power (each data point represents an extrapolation to zero microwave power). The example shown is for the alkene-coated, 2-inch-long, 1-inch-diameter, cylindrical cell filled with isotopically enriched ^{87}Rb [see Table I (row 7) and Fig. 4].

from ~100 nW to ~30 μW. For the cell filled with Rb with natural abundance we performed the measurements for each species.

For each microwave and optical power setting, we fit the light-transmission data to a Lorentzian and averaged the results from approximately five measurements. To mitigate frequency-calibration errors the center frequency was measured and averaged from the start of the scan and from the falling edge of the frequency marker-step [Fig. 3(a)]. The clock resonance width and frequency shift for each cell was extracted from a zero-microwave-power extrapolation followed by a zero-optical-power extrapolation [an example of light-power extrapolation is shown in Figs. 3(b)(1) and 3(b)(2)].

We measured the temperature dependence of the clock resonance width and frequency shift in one of the alkene-coated cells and found no significant dependence in a range of 24 to 31 °C. The range was limited by the alkene antirelaxation coating property, which was shown to deteriorate above 33 °C [12] and by the poor signal-to-noise ratio below 24 °C.

For consistency and for comparison with the results from Ref. [14], we repeated the clock resonance-frequency shift and width measurements in one of the paraffin-coated cells measured in that work (cell labeled H2 in Table I), and found equivalent results.

In all alkene-coated cells we found no significant dependence of the clock resonance width and frequency shift on whether the stem lock was open or closed. With the lock closed the vapor density was found to decrease over several hours (depending on the lock fit) due to the semipermanent absorption by the wall coating of the alkali-metal atoms (which could potentially be desorbed using the LIAD technique [35,36]). To improve and maintain a constant signal-to-noise ratio, all final measurements were made with the stem lock open. We note that the alkane-coated cells in Ref. [14] were not fitted with stem locks.

The clock resonance width and frequency shift measurements were scaled to the ^{85}Rb hyperfine transition frequency in a 1-in-diameter spherical cell at 25 °C. The scaling factors

TABLE I. Rows 1–5: Paraffin-coated-cell data from Ref. [14]. Rows 6 and 7–12: Deuterated-paraffin–coated-cell and alkene-coated cell data, respectively (this work). The work in Ref [14] includes the measurement of the Zeeman transverse relaxation time T_2 [also known as the nonlinear magneto-optical rotation (NMOR) coherence relaxation time] in three of the four cells used in that work. In the present work we measured the Zeeman longitudinal relaxation time T_1 using the technique described in Sec. V. The hyperfine resonance linewidth (scaled) $\gamma/(2\pi)$ and the frequency shift $\Delta\nu$ (scaled) are shown (in columns 10 and 11, respectively) scaled to the ^{85}Rb species in a 1-inch-diameter spherical cell, at 25 °C (Sec V). The alkane-coated-cell labeled "Gib" and the alkene-coated 4 inch cylindrical cell are filled with natural-abundance rubidium vapor.

Rb species	Cell shape	Cell size (in)	Temp. (°C)	$\bar{t}_c$[a] (μs)	Coating type (cell label [14])	T_1 (s)	T_2 (s)	Linewidth $\left(\frac{\gamma}{2\pi}\right)$[b] (Hz)	Linewidth $\left(\frac{\gamma}{2\pi}\right)$[c] (Hz)	Shift $\Delta\nu$[c] (Hz)
85	Sph.	4	25	249	Paraffin (Ale-10)		1.2	9.0	35	−96
85	Sph.	4	25	249	Paraffin (Gib)		2.9	4.3	44	−56
87			25	252				6.3	28	−74
87	Sph.	1.4	21	249	Paraffin (H2)		3.5	4.5	14	−57
87	Sph.	1.4	22	250	Paraffin (TTll)			3.7	14	−47
85	Sph.	1.2	33	73	Deuterated	0.8		11.3	50	−106
87	Cyl.	2 × 1	29	99	Alkene C20-24	3.0		57.1	37	−146
87	Cyl.	4 × 1	29	109	Alkene C20-24	4.2		47.7	33	−140
85			29	110				10.5	35	−132
87	Sph.	1.2	28	75	Alkene C20-24	17.7		26.1	17	−83
85	Sph.	1.2	29	74	Alkene C20-24	53		5.8	13	−68
85	Sph.	1.2	30	74	Alkene C30	1.6		7.6	19	−84

[a]Time between collisions.
[b]Calculated adiabatic and spin exchange contributions to the hyperfine resonance linewidth.
[c]Scaled experimental values (Sec. V).

were derived from the equations in Sec. III and include a cell geometric factor [Sec. III A and Eqs. (6) and (7)].

VI. RESULTS

One example of hyperfine resonance measurement is shown in Fig. 3(a). The selected example was one among several hundred other measurements used to derive the zero-power extrapolated hyperfine width and -frequency shift and exhibits a dispersive and wing residual in the hyperfine resonance data fit to a Lorentzian. A better fitting function would take into account the power broadening and the broader Gaussian (Doppler broadened) profile below the narrow near-Lorentzian "clock" resonance profile [14]. The near-Lorentzian profile originates from Dicke motional narrowing due to the cell size being comparable to the microwave wavelength. Imperfections in the measurement are the probable causes for the observed dispersive component. The corrections to the hyperfine frequency shift that would be derived from these imperfections are of the order of a few percent of the total frequency shift (itself of the order of 100 Hz) and fall within the measurement uncertainty.

The scaled (Sec. V) width and shift data, and the data from Ref. [14] on paraffin-coated cells, are summarized in Table I. The scaled hyperfine-linewidth data as a function of scaled frequency shift are plotted in Fig. 4(a). The Zeeman linewidth as a function of scaled hyperfine-frequency-shift data are plotted in Figs. 4(b) and 4(c).

There is good agreement between the data in Fig. 4(a), for the alkene-coated cells filled with ^{87}Rb, and the value predicted by the sum contribution (dotted line) of the spin exchange and adiabatic broadening mechanisms (Sec. III); however, we observe a 50% discrepancy for ^{85}Rb.

Comparing the results to those on alkane coatings [14], we find that the range of hyperfine frequency shifts is comparable (sightly larger) for cells coated with alkene than for cells coated with alkane. The Zeeman longitudinal relaxation rate $1/T_1$ of the C20-24 alkene-coated cells exhibit a linear dependence on the scaled frequency shift with a −66 Hz frequency offset [Fig. 4(c)]. The alkene C-30 and deuterated paraffin-coated cells data do not follow the same linear dependence, are not included in the fitting function [Fig. 4(c)], and are shown for comparison only.

The Zeeman linewidths $1/T_2$ (Zeeman transverse relaxation rate), which were measured for three of the four alkane coated cells [14] do not seem to exhibit such linear dependence [Fig. 4(b)]. In panel 4(b), we note that the $1/T_1$ (Zeeman longitudinal relaxation rate) data points [also shown in panel 4(c)], for the C-30 alkene- and deuterated-paraffin-coated cells, are within the same distribution as for the paraffin-coated-cell $1/T_2$ data.

VII. INTERPRETATION

A. Hyperfine resonance width and frequency shift

We have investigated the ground-state hyperfine transition in four C20-24 and one C-30 alkene-coated vapor cells. How do the results answer the question "Is long relaxation time due to a short wall-dwelling time?" and fulfill the motivation pertaining to the "application of alkali-metal-vapor-coated cells to a secondary frequency standard," introduced in Sec. I?

The alkene-coated cells do not have a smaller hyperfine transition frequency shift. If we assume that the average cell-wall adsorption energy is nearly constant and independent of the coating (Sec. III), then from Eqs. (1), (3), and (4), the alkene's long-lived Zeeman polarization property is not

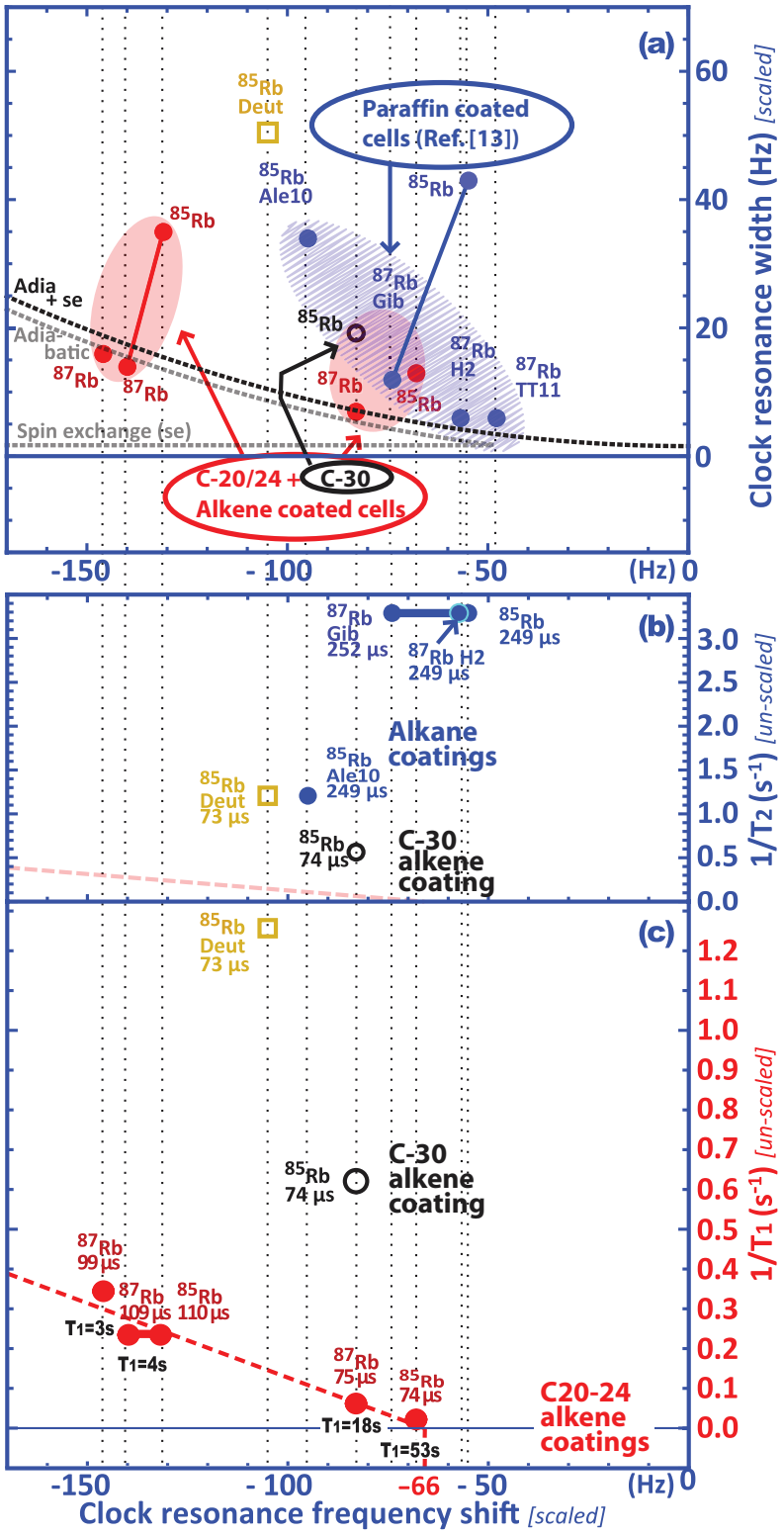

FIG. 4. (Color online) Panels (a), (b), and (c) show the data for the C-30 coated cell and for the deuterated-paraffin-coated cell as circles and squares respectively. The vertical dotted lines serve to guide the eye. Panel (a) shows the dependence of the scaled linewidth on the scaled-frequency shift of the hyperfine clock-resonance. The data are scaled (Sec. V) to a 1 inch spherical cell at 25 °C and to the hyperfine frequency of the ^{85}Rb species. The oval shapes serve to group cells with similar characteristics. The solid oval shows the alkene-coated cells with Zeeman polarization (longitudinal) relaxation times T_1 (Sec. V) ranging between 3 to 53 s. The hashed oval shows the paraffin coated cells [14]. The dashed lines are the simulated adiabatic, spin exchange, and sum of both contributions to the hyperfine-resonance linewidth. For panels (b) and (c), the time between wall collisions is given in μs for each cell. Typical error bar magnitudes are given in Fig. 3. The two horizontal segments join ^{85}Rb and ^{87}Rb data in the cells with rubidium in isotopic abundance. Note the different vertical-axis scales in (b) and (c). Panel (b) shows the dependence of Zeeman transverse relaxation rate $1/T_2$ on scaled-frequency shift of the hyperfine resonance for the three paraffin-coated cells of Ref. [14] for which T_2 was measured. The data points for the Zeeman longitudinal relaxation rate $1/T_1$, for the alkene C-30 and deuterated-paraffin coated cells, are added to panel (b) for reference only. The light slanted dashed line in panel (b) is the replica of the $1/T_1$ linear fit (darker dashed line) in panel (c). Panel (c) shows the dependence of Zeeman longitudinal relaxation rate ($1/T_1$) on scaled frequency-shift of the hyperfine resonance in the four alkene-coated cells in the present work. T_1 is indicated next to each alkene-coated cell in panel (c). The alkane C-30 and deuterated-paraffin-coated-cell data do not follow the same linear dependence observed in the alkene C20-24-coated cells and are not part of the linear fit in panel (c).

caused by a cell-wall dwelling time shorter than for the alkane coatings.

This results points to the possibility that the factor governing the difference in Zeeman relaxation in alkane and alkene-coated cells, is not the cell-wall dwelling time but is instead a smaller rms magnitude of the average fluctuations ΔE_w of the cell-wall adsorption energy E_w. Bouchiat and Brossel reached the same conclusion for alkane-coated cells [6].

A possible explanation for the cell-wall dwelling time being similar in alkene and alkane coatings is the curing process which is performed at ~60 °C and which is part of the manufacture of paraffin- and alkene-coated cells. During that process alkali-metal atoms are absorbed into and/or on

the coating. One may hypothesize that the alkene and alkane coatings are modified by the curing process to a final surface structure, which causes approximately the same cell-wall dwelling time, but has a different degree of uniformity.

Since the alkene-coating-induced clock resonance-frequency shift is not measured to be small, the coating's temperature dependence and stability will need to be assessed to determine whether alkene coatings offer an advantage for applications to secondary frequency standards.

The near-agreement between the scaled width of the clock resonance and the predicted value [dotted line in Fig. 4(a)] for the ^{87}Rb-filled cells, but not for the ^{85}Rb-filled cells, may be an artifact of the normalization step derived from Eqs. (8), (11), and (12). The near-50% discrepancy for ^{85}Rb could come from sources of relaxation that are additional to the adiabatic and spin exchange effects and fixed in nature, such as the stem effect. Fixed contributions make a relatively larger contribution to the scaled hyperfine resonance width of ^{85}Rb, whose hyperfine frequency is approximately half that of ^{87}Rb (the scaling factor is quadratic in the ratio of the hyperfine frequencies).

B. Zeeman relaxation and hyperfine resonance frequency shift

The results in Sec. VI show that alkane and alkene coatings have comparable hyperfine frequency shift, leading to the conclusion that the up-to-two orders of magnitude longer Zeeman relaxation time of the alkene coatings was not caused by a shorter cell-wall dwelling time [Eqs. (3) and (4)]. However, in the four C20-24 alkene-coated cells (which have comparable geometric factors), we observe that within the range of hyperfine frequency shifts there appears to be a linear dependence on the Zeeman linewidth [Fig. 4(c)]; this means that in alkene-coated cells the wall-dwelling time $\bar{t}_w$ plays a role in determining the Zeeman linewidths of the cells. A similar linear dependence has not been observed for alkane-coated cells [14]. This may be due to the homogeneity of the history and manufacture of the alkene cells (prepared following the procedure described in Ref. [12], within a few-month period), in contrast to the history of the four alkane cells in Ref. [14] (manufactured over several decades and coated by different techniques).

Bouchiat and Brossel also inferred, from their observations in alkane-coated cells, a near-linear dependence of the Zeeman linewidth $1/T_1$ on the wall-dwelling time $\bar{t}_w$ [6],

$$\frac{1}{T_1} \propto \frac{\bar{t}_w}{\bar{t}_w + \bar{t}_c} (H_o)^2 , \tag{13}$$

where H_o is the rms amplitude of the magnetic-field fluctuation on the surface as "seen" by the alkali-metal atoms.

If we assume that ΔE_{hf} does not vary significantly from cell to cell (as assumed in Sec. III), one may apply the linear relationship $1/T_1 \propto \Delta\nu$ [Eqs. (13) and (8)] to a family of cells, which explains the results in the four alkene-coated cells in this work. We conclude that, within the constraint stated above, a shorter wall-dwelling time $\bar{t}_w$ in alkene-coated cells is related to a narrower Zeeman linewidth $1/T_1$ as shown in Fig. 4(c).

We also observe that the characteristics of the cell with 53 s Zeeman relaxation time (Table I) is equivalent to a hypothetical "perfect coating" combined with one ring-shaped gap between the cell volume and the cell reservoir through an imperfectly fitted stem lock. A 2.3-μm-wide, 2-mm-diameter gap circumscribing the stem lock through which we assume the alkali-metal atoms reach the cell reservoir (which scrambles the atoms' atomic polarization) is approximately equivalent (at room temperature) to a 53 s Zeeman relaxation time. We may then interpret the -66 Hz offset [Fig. 4(c)] as being the hyperfine frequency shift corresponding to the minimum cell-wall adsorption time $\bar{t}_w$ and to near-zero Zeeman linewidth, and corresponding to the characteristics of an ideal alkene coating. An expanded interpretation of the results is found in Chap. 4 of Ref. [38].

VIII. CONCLUSION

We have investigated the frequency shift and width of the ground-state hyperfine transition in four C20-24 alkene-coated cells and compared the results with those in four alkane-coated cells [14]. We found a comparable frequency shift with alkene and alkane cells, which implies comparable cell-wall dwelling time. In alkene-coated cells we also observed a linear dependence of the Zeeman linewidths on the hyperfine frequency shift (equivalent to the cell-wall dwelling time), a dependence which was not observed in the alkane-coated cells. The linear dependence has a -66 Hz offset in a 1-inch spherical alkene-coated cell, (at 25 °C) filled with a ^{85}Rb vapor; the cell-wall dwelling time corresponding to this frequency offset may be the one in an ideal coating having near-zero Zeeman linewidth. In alkene-coated cells the association of shorter wall-dwelling times and narrower Zeeman linewidths may shed new understanding on the surface dynamics governing the interaction of alkali-metal atoms and alkene coatings.

ACKNOWLEDGMENTS

The authors are specifically thankful to Svenja Knappe and to Leo Hollberg (formerly at NIST) for insightful exchanges by email and for the extended loan of a microwave generator, central to the apparatus in this work. We are also grateful to M. Bouchiat, S. Seltzer, M. Ledbetter, S. Pustelny, V. M. Acosta, A. Shmakov, B. Patton, K. Tsigutkin, K. Jensen, D. Dounas-Frazer, D. English, A. Jarmola, N. Leefer, A. Park, and G. Iwata for helpful discussions. This work was supported by NSF (Grant No. PHY-0855552) and by the US Department of Energy through the LBL Nuclear Science Division (Contract No. DE-AC03-76SF00098).

[1] D. Budker, W. Gawlik, D. F. Kimball, S. M. Rochester, V. V. Yashchuk, and A. Weis, Rev. Mod. Phys. **74**, 1153 (2002).
[2] D. Budker and M. Romalis, Nat. Phys. **3**, 227 (2007).
[3] S. Pustelny, D. F. Jackson-Kimball, S. M. Rochester, V. V. Yashchuk, and D. Budker, Phys. Rev. A **74**, 063406 (2006).
[4] N. Ramsey, Rev. Sci. Instrum. **28**, 57 (1957).

[5] H. G. Robinson, E. S. Ensberg, and H. G. Dehmelt, Bull. Am. Phys. Soc. **3**, 9 (1958).
[6] M. A. Bouchiat and J. Brossel, Phys. Rev. **147**, 41 (1966).
[7] M. A. Bouchiat, Ph.D. thesis, École Normale Supérieuere, Paris, 1964.
[8] S. J. Seltzer, D. J. Michalak, M. H. Donaldson, M. V. Balabas, S. L. Barber, S. K. Bernasek, M.-A. Bouchiat, A. Hexemer, A. M. Hibberd, D. F. Jackson Kimball, C. Jaye *et al*., J. Chem. Phys. **133**, 144703 (2010).
[9] S. J. Seltzer, D. M. Rampulla, S. Rivillon-Amy, Y. J. Chabal, S. L. Bernasek, and M. V. Romalis, J. Appl. Phys. **104**, 103116 (2008).
[10] G. Castagna, G. Do Domenico, A. Hofer, P. Knowles, C. Macchione, and A. Weiss, Appl. Phys. B: Lasers Opt. **96**, 763 (2009).
[11] M. V. Balabas, K. Jensen, W. Wasilewski, H. Krauter, and L. S. Madsen, Opt. Express **18**, 5825 (2010).
[12] M. V. Balabas, T. Karaulanov, M. P. Ledbetter, and D. Budker, Phys. Rev. Lett. **105**, 070801 (2010).
[13] C. Rahman and H. G. Robinson, J. Quantum Electron. **QE-23**, 452 (1987).
[14] D. Budker, L. Hollberg, D. F. Kimball, J. Kitching, S. Pustelny, and V. V. Yashchuk, Phys. Rev. A **71**, 012903 (2005).
[15] In this work we follow the approach by J. Vanier and C. Audoin.
[16] J. Vanier and C. Audoin, *The Quantum Physics of Atomic Frequency Standards* (Adam Hilger, Bristol/Philadelphia, 1989).
[17] M. Stephens, R. Rhodes, and C. Weiman, J. Appl. Phys. **76**, 3479 (1994).
[18] M. V. Romalis and L. Lin, J. Chem. Phys. **120**, 1511 (2004).
[19] J. H. de Boer, *The Dynamical Character of Adsorption*, 4th ed. (Clarendon, Oxford, 1968).
[20] P. Clausing, Ann Phys. **7**, 489 (1930).
[21] P. Clausing, Ph.D. thesis, University of Leiden, Netherlands, 1928.
[22] V. Liberman and R. J. Knize, Phys. Rev. A **34**, 5115 (1996).
[23] J. Brewer, V. G. Bordo, M. J. Kasprowicz, and H.-G. Rubahn, Phys. Rev. A **69**, 062902 (2004).
[24] M. Meucci, E. Mariotti, P. Bicchi, C. Marinelli, and D. L. Moi, Europhys. Lett. **25**, 639 (1994).
[25] S. Gozzini, A. Lucchesini, L. Marmugi, and G. Postorino, Eur. Phys. J. D **47**, 1 (2008).
[26] T. Karaulanov, M. T. Graf, D. English, S. M. Rochester, Y. Rosen, K. Tsigutkin, D. Budker, M. V. Balabas, D. F. Jackson Kimball, F. A. Narducci *et al*., Phys. Rev. A **79**, 012902 (2009).
[27] K. F. Zhao, M. Schaden, and Z. Wu, Phys. Rev. Lett. **103**, 073201 (2009).
[28] E. Ulanski and Z. Wu, Appl. Phys. Lett. **98**, 201115 (2011).
[29] M. V. Balabas and O. Y. Tret'yak, Tech. Phys. **57**, 1257 (2012).
[30] M. V. Balabas and S. G. Przhibel'skii, Chem. Phys. Rep. **14**, 882 (1995).
[31] H. N. de Freitas, M. Oria, and M. Chevrollier, Appl. Phys. B **75**, 703 (2002).
[32] X. Zhang, M. Yu, C. T. M. Kwok, R. Vaidyanathan, R. D. Braatz, and E. G. Seebauer, Phys. Rev. B **74**, 235301 (2006).
[33] H. Margenau, P. Fontana, and L. Klein, Phys. Rev. **115**, 87 (1959).
[34] W. Happer, Rev. Mod. Phys. **44**, 169 (1972).
[35] M. T. Graf, D. F. Kimball, S. M. Rochester, K. Kerner, C. Wong, D. Budker, E. B. Alexandrov, M. V. Balabas, and V. V. Yashchuk, Phys. Rev. A **72**, 023401 (2005).
[36] A. Shmakov, T. Karaulanov, M. V. Balabas, S. M. Rochester, S. Pustelny, and D. Budker (unpublished).
[37] V. V. Yashchuck, D. Budker, and J. R. Davis, Rev. Sci. Instrum. **71**, 341 (2000).
[38] E. P. Corsini, Ph.D. thesis, University of California, Berkeley, US, 2012.
[39] E. B. Alexandrov, M. V. Balabas, D. Budker, D. S. English, D. F. Kimball, C.-H. Li, and V. V. Yashchuk, Phys. Rev. A **66**, 042903 (2002).
[40] W. Franzen, Phys. Rev. **115**, 850 (1959).